Cellulose (2020) 27:8215–8235
https://doi.org/10.1007/s10570-020-03352-x

ORIGINAL RESEARCH

Batch and column adsorption of cations, oxyanions and dyes on a magnetite modified cellulose-based membrane

Jovana Perendija · Zlate S. Veličković · Ilija Cvijetić · Jelena D. Rusmirović · Vukašin Ugrinović · Aleksandar D. Marinković · Antonije Onjia

Received: 1 April 2020 / Accepted: 12 July 2020 / Published online: 20 July 2020

Abstract An optimized method is presented to make magnetite (MG) modified cellulose membrane (Cell-MG) from 3-aminopropyltriethoxysilane and diethylenetriaminepentaacetic acid dianhydride functionalized waste cell fibers; (Cell-NH_2 and Cell-DTPA), and amino-modified diatomite. Functionalized Cell-NH_2, Cell-DTPA fibers, and diatomite were structurally and morphologically characterized using FT-IR, Raman, and FE-SEM analysis. Amino and carboxyl group content was determined via standard volumetric methods. Response surface method was applied to rationalize the number of experiments related to Cell-MG synthesis and heavy metal ions column adsorption experiments. The effects of pH, contact time, temperature, and initial concentration of pollutants on adsorption and kinetics were studied in a batch, while initial concentration and flow rate were studied in a flow system. The calculated capacities of 88.2, 100.7, 95.8 and 78.2 mg g^{-1} for Ni^{2+}, Pb^{2+}, Cr(VI) and As(V) ions, respectively, were obtained from Langmuir model fitting. Intra-particle diffusion as a rate-limiting step was evaluated from pseudo-second-order and Weber–Morris model fitting. Thermodynamic parameters indicated spontaneous and low endothermic processes. The results from reusability study, wastewater purification and fixed-bed column study proved the high applicability of Cell-MG. Additionally, high removal capacity of four dyes together with density functional theory and molecular interaction fields, help in the establishment of relation between the adsorption performances and contribution of non-specific and specific interactions at adsorbate/adsorbent interface.

Electronic supplementary material The online version of this article (https://doi.org/10.1007/s10570-020-03352-x) contains supplementary material, which is available to authorized users.

J. Perendija
University of Belgrade, Institute of Chemistry, Technology and Metallurgy, National Institute of the Republic of Serbia, Center of Ecology and Technoeconomics, Njegoševa 12, 11001 Belgrade, Serbia
e-mail: j.nikolic.ihtm@tesla.rcub.bg.ac.rs

Z. S. Veličković
Military Academy, University of Defense, Generala Pavla Jurišića Šturma 33, 11000 Belgrade, Serbia
e-mail: zlatevel@yahoo.com

I. Cvijetić
Faculty of Chemistry, Innovation Center, University of Belgrade, Studentski trg 12, 11000 Belgrade, Serbia
e-mail: ilija@chem.bg.ac.rs

J. D. Rusmirović · V. Ugrinović
Innovation Center, Faculty of Technology and Metallurgy, Karnegijeva 4, 11120 Belgrade, Serbia
e-mail: jrusmirovic@tmf.bg.ac.rs

Graphic abstract

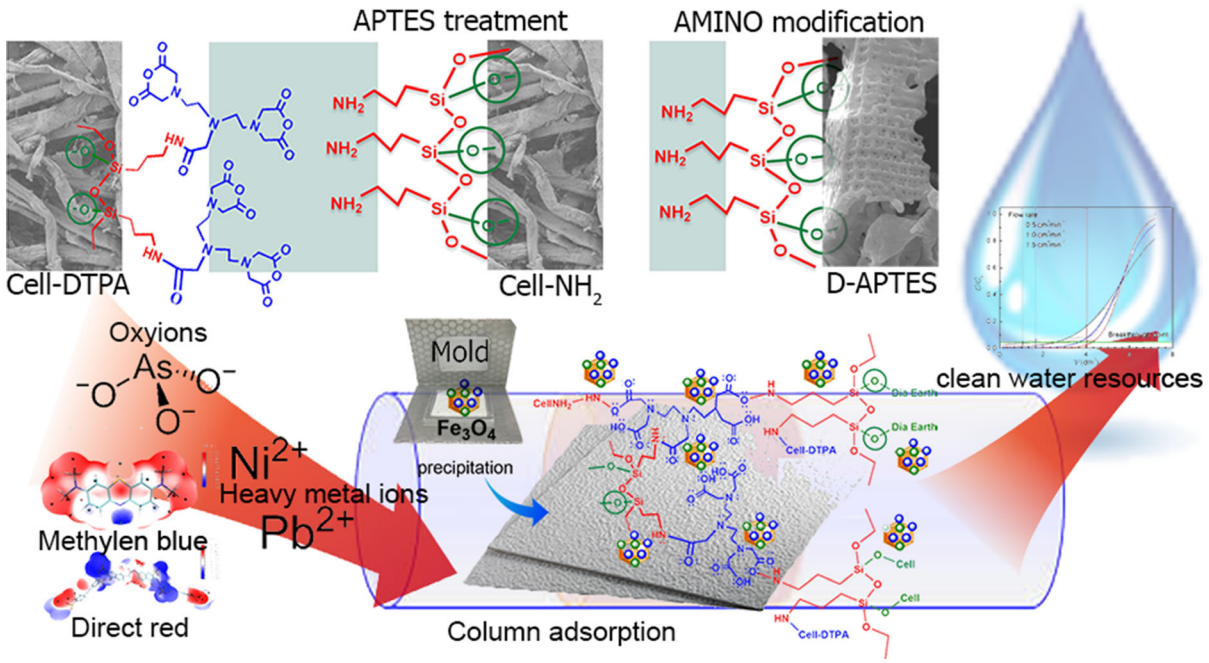

Keywords Cellulose membrane · Magnetite · Batch adsorption · Fixed-bed column adsorption study · Pollutant

Introduction

Pollution of water systems from the various sources is one of the most significant problems of humanity over the past decades. Water pollution is mainly caused by organic pollutants and heavy metal ions (Sun et al. 2013; Pramanik et al. 2019). This is the reason for a number of changes in water quality, whereby dying of aquatic living world occurs as a consequence. Heavy metal ions are considered to be a group of stable pollutants that are non-biodegradable, highly toxic and accumulable in the food chain. When their concentration exceeds the permissible limit in the environment, that may pose a serious threat to human health (Vadakkekara et al. 2019). Many studies have been conducted with the aim of finding and improving materials that can reduce the concentration of heavy metals in water to a minimum (Dave and Chopda 2014; Arantes et al. 2017; Fakhre and Ibrahim 2018).

Adsorption process provides flexibility and simplicity in operation. The important advantages of adsorption over conventional methods are: high efficiency, low cost, regeneration of adsorbents and possibility of metal recovery. Metal oxides, including ferric oxides, are economical adsorbents for the removal of heavy metal ions from wastewater due to large surface area, small particle size, magnetism, high capacity and selectivity (Tang and Lo 2013; Nouri and Marjani 2019). However, metal oxides are prone to agglomeration, which significantly reduces their capacity and selectivity (Nouri and Marjani 2019). The design of hybrid materials obtained by impregnation of porous carriers with magnetite (MG) enables the preservation of important properties of ferric oxide

V. Ugrinović
e-mail: vugrinovic@tmf.bg.ac.rs

J. D. Rusmirović
Military Technical Institute, Ratka Resanovića 1, 11000 Belgrade, Serbia

A. D. Marinković (✉) · A. Onjia
Faculty of Technology and Metallurgy, University of Belgrade, Karnegijeva 4, 11060 Belgrade, Serbia
e-mail: marinko@tmf.bg.ac.rs

A. Onjia
e-mail: onjia@tmf.bg.ac.rs

(Hua et al. 2012; Xu et al. 2012; Tkacheva et al. 2013). Recently, the emphasis is on the use of natural materials, due to their low price and a large potential for the improvement of adsorption properties through structural modifications (O'Connell et al. 2008; Li et al. 2020).

Cellulose is an extremely attractive raw material, owing to the biodegradability, bio-renewability and biocompatibility (El Achaby et al. 2017). Unmodified cellulose has low adsorption capacity and variable physical stability. Thus, chemical modification of cellulose can be carried out to achieve an adequate durability and increased adsorption capacity (Kamel et al. 2006). The chemical modification of cellulose hydroxyl groups makes it possible to improve the adsorption capacity of the material, and therefore the cellulose is ideal as a support for surface modifications (Rafieian et al. 2019; Han et al. 2020). The introduction of carboxylic and terminal amino groups provides an effective way for precipitation of ferric oxides (Sun et al. 2014; Luo et al. 2016; Arantes et al. 2017).

A small number of studies have been conducted to investigate cellulose-diatomite materials. Diatomite is a widespread, low-cost material, with high porosity, high permeability, small particle size, large surface area, and low thermal conductivity. The surface of diatomite particles has strong negative charges, therefore diatomite is suitable for the adsorption of heavy metal ions (Khraisheh et al. 2004; Sheng et al. 2009; ElSayed 2018; Salih and Ghosh 2018).

The aim of this study was to develop cost-effective MG modified cross-linked cellulose adsorbent/membrane used for the removal of oxyanions and heavy metal ions (Li et al. 2014, 2017). Production technology was based on amino/anhydride system reactivity in the course of membrane moulding at such molar ratio to produce a significant amount of carboxylic groups as the active centres for iron-binding. Thus, the obtained membrane is a suitable matrix for precipitation of magnetite, which increases the adsorption performances. Solvent/nonsolvent system was applied for controllable impregnation of MG. The second objective was to evaluate and model the performance of the cation and oxyanion removal from aqueous solution and wastewater in relation to: (1) adsorption capacity, (2) kinetic and activation parameter determination, (3) kinetic study, (4) adsorption performances in a dynamic system to analyze the effect of flow rate (i.e., residence time) and inlet concentration on the capacities. Hydrodynamic properties and membrane applicability were considered with respect to rejection efficiency and membrane absorptivity concerning selected dyes.

Experimental part

Chemicals and materials

Details on chemicals and materials being used are given in Supplementary material.

Synthesis of dianhydride of diethylenetriaminepentaacetic acid

Synthesis of bis(2-(2,6-dioxomorpholino)ethyl)glycine, i.e. (diethylenetriaminepentaacetic acid dianhydride; DTPA) was described in Supplementary material.

Pre-treatment of cellulose fibres (Cell)

Different methods used for pre-treatment of cellulose fibres (Cell), and selection of optimal method are given in Supplementary material.

Procedure for preparation of amino-functionalized Cell fibres (Cell-NH_2) and diatomaceous earth (D-APTES)

Detailed procedure for amino-functionalization of Cell fibres and diatomaceous earth is presented in Supplementary material.

Procedure for the preparation of Cell-DTPA fibres

The prepared Cell-NH_2 (10 g) was washed with 50 cm^3 of pyridine, immersed in a mixture containing 50 cm^3 of DMSO and 50 cm^3 of pyridine and treated by DTPA dianhydride (2.5 g) in a three-necked 250 cm^3 round-bottom flask, which was fitted with a thermometer, a reflux condenser and a N_2 gas inlet tube. The mixture was heated at 60 °C for 24 h under N_2. The Cell-DTPA product was filtered, washed with dry tetrahydrofuran and stored in a desiccator under N_2.

The Cell-COOH filter membrane preparation

The optimization method concerning the quantity of Cell-DTPA and D-APTES was applied to obtain mechanical/hydrodynamic and adsorption properties of Cell-COOH membrane. A simple method was used for membrane preparation: 8.5 g of Cell-DTPA and 1 g of Cell-NH_2 was finely distributed in 50 cm^3 dry DMF under mechanical mixing (500 rpm) for 15 min, under nitrogen. Dry D-APTES (0.5 g) was added into the reactor and the process was continued for 30 min at 15–20 °C. Filtration of the material, using cellulose membrane 0.22 μm, was performed without vacuum to prepare layered structure (5 mm thick) until no dripping of solvent was achieved. After 2 h of drying at room temperature, the prepared membranes were pressed between porous aluminum plates (0.2 mm) in a compression-molding machine with a load of 20–30 kN with heating (80 °C) to obtain compact material as a result of cross-linking reactions (amide bond formation).

Three-step method of Cell-MG hybrid membrane preparation

Cell-COOH membrane (10 g) was soaked with xylene (100 cm^3) in a glass vessel with gas inlet/outlet valves. In a continuous flow of N_2 through two-phase system xylene/Cell-COOH slow addition (15 min) of the 20 cm^3 (0.26 mol dm^{-3}) of $FeSO_4{\cdot}7H_2O$ solution, was performed. Optimization of Cell-MG hybrid membrane synthesis was performed with respect to final pH and concentration of $FeSO_4{\cdot}7H_2O$. According to preliminary results, the optimal procedure was established as follows: MG precipitation was performed by continual stream of N_2 at 90 °C, and by drop-wise addition of an oxygen-free solution of 10 cm^3 (0.1173 g KNO_3 and 0.870 g KOH) for 20 min (2 min addition/1 min ultrasound—Bandelin 20 kHz) into the dispersion of xylene/Cell-COOH impregnated with $FeSO_4{\cdot}7H_2O$. The reaction mixture was heated at 90 °C for 60 min and left overnight until the completion of crystallization. The obtained adsorbent Cell-MG hybrid black membrane was washed with deionized water (DW) and subjected to freeze/drying process (analogously to the method given in "Pre-treatment of cellulose fibres (Cell)" section). For comparative purpose, a three-step procedure was applied using 20 cm^3 (87 mmol dm^{-3}) of $FeSO_4{\cdot}7H_2O$, and 10 cm^3 (39 mg KNO_3 and 290 mg KOH) in a similar manner.

Characterization of adsorbents

Full details on characterization methods are given in Supplementary material.

Batch adsorption experiments

Adsorption experiments, performed in a batch system, related to adsorption and kinetic study, are presented in Supplementary material.

Bed column experiments

Adsorption experiments, performed in a bed column system, related to adsorption and kinetic study, are presented in Supplementary material.

Response surface methodology (RSM): experimental design of adsorbent preparation

The applied RSM methodology is presented in Supplementary material.

Measurement of membrane permeability

Cell-COOH and Cell-MG membranes were subjected to water permeability experiments. The experimental set-up for a cross-flow filtration is given in Fig. S1.

Calculation of molecular electrostatic potential (MEP) and interaction fields (MIF)

All details on the computation of MEP and MIF for studying the adsorbent/adsorbate interactions of 4 dyes (methyl orange—MO, methylene blue—MB, Reactive black 5—RB5 and Direct Red 80—DR80) are given in Supplementary material.

Results and discussion

In the first step, adsorption performance of selected building material was considered (Table S4), and it was evident that both non-modified diatomite and cellulosic materials showed low adsorption capacity. Thus, the main goal of this study was to produce

highly functionalized porous membranes with concomitant low decrease of mechanical properties (tensile strength) and good hydrodynamic properties.

Design of adsorption experiments using RSM methodology

Graphical representation of the optimization of Cell-DTPA filter media production, output variable, i.e. content of carboxyl group, with respect to the quantity of D-APTES and Cell-DTPA is shown in Fig. 1a. Graphical area with intense red colour designates region that meets critical properties. More precise optimization conditions are obtained by point prediction through the software based on the factors or components included in the model. The operational values of the selected variables are shown in Tables S1 and S2, together with the experimental design, which included 16 experimental runs with five repetitions. The output variables were carboxyl group content in Cell-COOH and Ni^{2+} capacity on Cell-MG, $q_{e[Ni^{2+}]}$. Experimental data were fitted with a second-order polynomial equation using commercial software. Full details on statistical analysis are given in Supplementary material.

An optimization procedure relates to achieving appropriate carboxyl content (Fig. 1a) and Ni^{2+} removal capacity (Fig. 1b) as well as attainment of satisfactory membrane porosity, mechanical and dimensional stability to be applicable in a high flux flow system. Improvement of MG precipitation method (Fig. 1b), in relation to one step process, was achieved by three-step addition of $FeSO_4$ solution that provided uniform and porous MG deposit with high adsorption capacity. The optimal operational parameters for the synthesis of Cell-COOH (Fig. 1a) are presented in "The Cell-COOH filter membrane preparation" section, while the optimal MG precipitation procedure (Fig. 1b) is given in "Three-step method of Cell-MG hybrid membrane preparation" section. Also, freeze-drying method gave a 12% higher adsorption capacity compared to the classical vacuum drying method. The porosity, amino and carboxyl group's content, and point of zero charge, i.e. pH_{PZC}, of synthesized materials are given in Table 1.

Amino value and carboxyl content changes (Table 1), in the course of transformation, reflect the successfulness of Cell fibre modification. Results of Cell-MG synthesis indicated a good affinity of Cell-COOH surface to MG deposit. AAS analysis of the Cell-MG hybrid membrane nitric acid extracts indicated introduction of 7.8 wt% of iron, i.e. ~ 10.8 wt% of MG. Analogously to Cell-MG synthesis ("Characterization of adsorbents" section), Cell-NH_2-MG was prepared from Cell-NH_2 at 6.2 wt% MG loading, thus achieving 42% and 51% lower capacities with respect to Cr(VI) and As(V). It means that branching of side-group, by using DTPA, introduces high-affinity carboxyl group, which, together with a residual amino group (Table 1) provides effective initial iron ion coordination sites and subsequent MG crystallization. Good accordance of the results of porosity determination and image analysis confirm membrane porosity consisting mainly from large pore size (sub-micrometer to tenth μm range). Also, the capacity of Cell-MG, obtained by one-step synthesis, is 32% lower (at 7.4 wt% of MG loading). In general, the presented results highlight the significance of the optimization procedure applied to obtain desirable material performances at the lowest number of experiments performed. An overall process of Cell-MG production starting from the waste cellulosic fiber is presented in Fig. 2.

Characterization of the adsorbent

Mechanical properties

One of the important prerequisite for the use of membrane material in a water purification is mechanical strength. Due to this, membranes from Cell, Cell-NH_2, and Cell-DTPA were prepared analogously to the procedure given for Cell-MG ("Three-step method of Cell-MG hybrid membrane preparation" section), and used for studying the changes in mechanical properties in relation to the influences of the strength of covalent binding/intermolecular interactions. The stress–strain plots of Cell, Cell-NH_2, Cell-COOH and Cell-MG membrane are shown in Fig. S3, and the corresponding data are provided in Table 2.

The data show a slight decrease in stress at the break and maximal strain when cellulose fibres are functionalized with APTES, which indicates the significance of hydrogen bonding to membrane compactness/strength. Lower strength of hydrogen bonding in Cell-NH_2, including main bonding of NH_2 and OH groups in comparison to OH-OH hydrogen bonding in Cell fibres, causes both stress at break

and maximum strain decrease of 6.3% and 0.7%, respectively. The increase of stress at break and maximum strain is observed for Cell-COOH membrane (11.6%), while loading of MG contributes to the membrane strength decrease of 14.7% with respect to Cell fibres. Somewhat increased stress at break, noted for Cell-COOH, could be the result of increased cross-linking, i.e. both covalent bonding and longer and flexible grafting fragment are able to establish more effective hydrogen bonding between carboxylic groups. Stress at break decrease in Cell-MG hybrids is of complex nature due to opposite influence of precipitated Fe_3O_4 and strengthening effect, and partial breaking of hydrogen bonding. The mechanical strength of the wet membrane showed a similar trend, and 6 and 15 times lower stress at break for Cell-MG and Cell-COOH, respectively. The lower mechanical properties of wet Cell-COOH arise from disruption of hydrogen bonding between hydrophilic functionalities, i.e. carboxylic group, thus causing failure of intermolecular chain interactions. The low elongation of all samples as a result of the breakage of intermolecular hydrogen bonds causes defibrillation/tearing without structural arrangement/reinforcement. The diversity of the literature data on mechanical strength of cellulose-based membrane is discussed in Supplementary material.

Thermogravimetric (TGA) and XRD analysis

TGA analysis was applied to study the thermal behaviour of synthesized samples, and obtained results are given in Fig. 3a. The percentage weight residues were 13.81%, 15.84%, 19.01% and 33.02% for the Cell fibre, Cell-NH_2, Cell-DTPA and Cell-MG, respectively (Fig. 3a). The percentage of the residue (33.02%) is indicative of the amount of diatomite and magnetite incorporated into the Cell-MG hybrid adsorbent. The Cell, Cell-NH_2 and Cell-DTPA fibres decompositions occur in three steps: the first mass loss in the TGA curves starting at $\sim$ 50 °C is attributed to a significant amount of water released from the Cell, Cell-NH_2 and Cell-DTPA fibres. The second decomposition occurs in three steps: at various temperatures with the initial point originated in the range from 200 to 400 °C, and is assigned to the modified cellulose thermal degradation with the main endothermic peak in the DTA curve around 350 °C (results are not presented). The higher stability of Cell-MG is due to the protection of MG cover layer on modified Cell fibre.

XRD pattern of Cell-MG hybrid membrane is given in the Fig. 3b, and XRD pattern of cellulose is shown in Supplementary material (Fig. S4). Diffraction peak at $2\theta = 22.0^\circ$ is attributed to the plane of cellulose fibre. The analysis showed the presence of diatomite with the typical crystalline diffraction peak at $2\theta = 22.0^\circ$, which corresponded to values for the (101) planes of SiO_2 (JCPDS Card No. 39-1425) (Lu et al. 2017). The XRD pattern of the sample showed the characteristic peaks at 30.3°, 35.73°, 37.0°, 43.17°, 54.7°, 57.10°, 63.0°, 74.9° (JCPDS 19–629), which confirmed the presence of magnetite. The characteristic peaks at $2\theta = 21.2^\circ$, 26.3° 33.1°, 38.9°, 40.9°, 53.7° corresponded to amorphous goethite (ICDD PDF2 No. 81-0464).

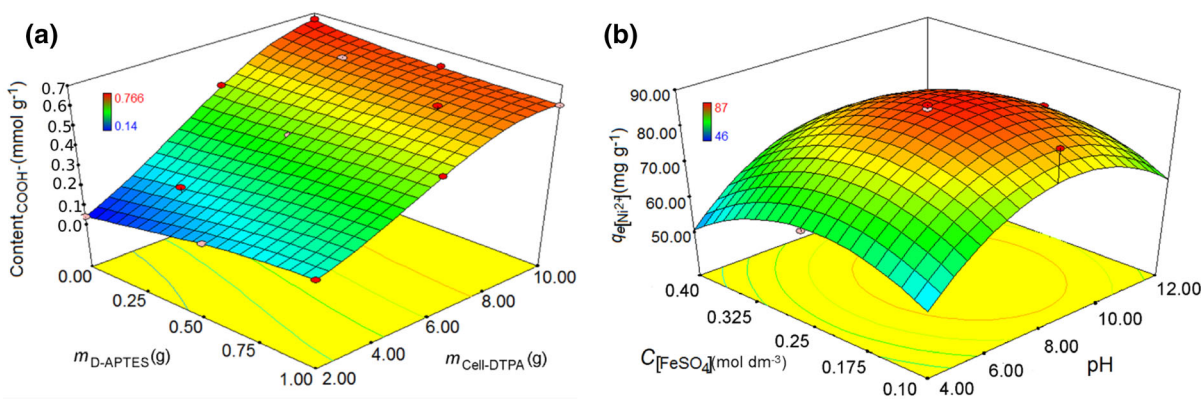

Fig. 1 Contour diagrams representing the relation between (**a**) carboxyl group content in Cell-COOH versus mass of D-APTES and Cell-DTPA (Table S1), and (**b**) Ni^{2+} capacity on Cell-MG, $q_{e[Ni^{2+}]}$, versus pH and $C_{[FeSO_4]}$ (Table S2)

Table 1 Porosity, amino and carboxyl group's content, and pH_{PZC} of synthesized materials

Material/properties	Porosity[a]	Amino value[b] μmol g^{-1}	Carboxyl content μmol g^{-1}	pH_{PZC}	
Cell	–	–	–	4.0	
Cell-NH_2	–	780	–	5.8	
Cell-DTPA	–	340	874	3.9	
Cell-COOH membrane	65	560	680	4.4	
Cell-MG hybrid membrane	58	12	23	6.6[c]	6.2[c]

[a]Image analysis was used for porosity determination (Supplementary material)

[b]D-APTES – 5 mmol g^{-1}

[c]pH_{PZC} before (6.6) and after As(V) adsorption (6.2)

FTIR and Raman spectroscopy

FTIR and Raman techniques were used to monitor the introduction of surface functionalities, i.e. successfulness of material modification.

The FTIR spectra of Cell, Cell-NH_2, Cell-DTPA fibres and Cell-MG hybrid membrane are shown in Fig. 4a, while for D-APTES in Supplementary material. As can be seen from the adsorbent spectrum, the strong adsorption at 3430 cm^{-1} occurs as a result of the stretching of the O–H and Si–OH groups and is overlapping with the symmetric vibrations of the N–H group in Cell-NH_2. The adsorption at 2922 and 2853 cm^{-1} is due to the valence C–H stretching vibration (Munajad et al. 2018), and the range of 1640–1384 cm^{-1} is attributed to the bending mode of C–H groups derived from cellulose. A band at 1090 cm^{-1} indicates the presence of Si–O-Si from siloxane and with a major contribution of C–O groups in a cellulose polysaccharide skeleton (Ren et al. 2017). After the modification process, the spectral bands shift due to the introduction of new functional groups. The major changes were observed in the modification of the Cell fibre with APTES, and subsequent modification with MG, which led to the appearance of peaks at 1508 and 574 cm^{-1}, originating from N–H and Fe–O groups, respectively (Ahangaran et al. 2013; Boyatzis et al. 2016).

Raman spectra of Cell, Cell-NH_2, Cell-DTPA and Cell-MG hybrid membrane are shown in Fig. 4b. The band observed in the region over 3000 cm^{-1} in Raman spectrum of Cell (Fig. 4b), originates from δ(O–H) stretching vibrations (Szymańska-Chargot et al. 2011). The intensity of δ(O–H) stretching band decreases in the Raman spectrum of Cell-NH_2, and disappears in further modification steps (Raman spectra of Cell-DTPA and Cell-MG). In the Cell-NH_2 Raman spectrum, the δ(O–H) stretching band is overlapped with bands that originate from NH stretching vibration, ν(NH) (Freire et al. 2017). The characteristic peak at 2889 cm^{-1} observed in all filter samples originates from C–H and CH_2 stretching of cellulose (Wiley and Atalla 1987). In the 1317–1477 cm^{-1} region, bending vibrations of δ(CH_2), δ(HCC), δ(HCO) and δ(COH) are predominant and appeared in Raman spectra of all cellulose membranes (Wiley and Atalla 1987; Szymańska-Chargot et al. 2011). The cellulose band of medium-strong intensity at ∼ 1096 cm^{-1} is assigned to the CC and CO stretching motions and some amounts of HCC and HCO bending of glycosidic bonds (Szymańska-Chargot et al. 2011; Vítek et al. 2017). The intensity of this peak decreases after three steps of modification, indicating the structural changes in the modified Cell-NH_2 and Cell-DTPA fibres. The bands observed in the region around 1000 cm^{-1} are assigned as stretching of CN, ν(CN) (Freire et al. 2017). The medium intensity peak observed in region 1720–1740 cm^{-1} corresponds to C = O group vibration from DTPA moieties. Comparing the Cell, Cell-NH_2 and Cell-DTPA Raman spectra with the spectrum of the Cell-MG hybrid, broadening and loss of resolution of the spectrum could be observed. This would suggest that the microcrystalline structure of cellulose is destructed with chemical modification and that magnetite nanoparticles cover cellulose fibres. From the non-polarized spectrum of Cell-MG hybrid, the magnetite predicted phonon bands appear as a characteristic peak at 670 cm^{-1} (Shebanova and Lazor 2003). The peaks below 500 cm^{-1} originate from the diatomite (SiO_2) stretching vibration (Popovic et al. 2011).

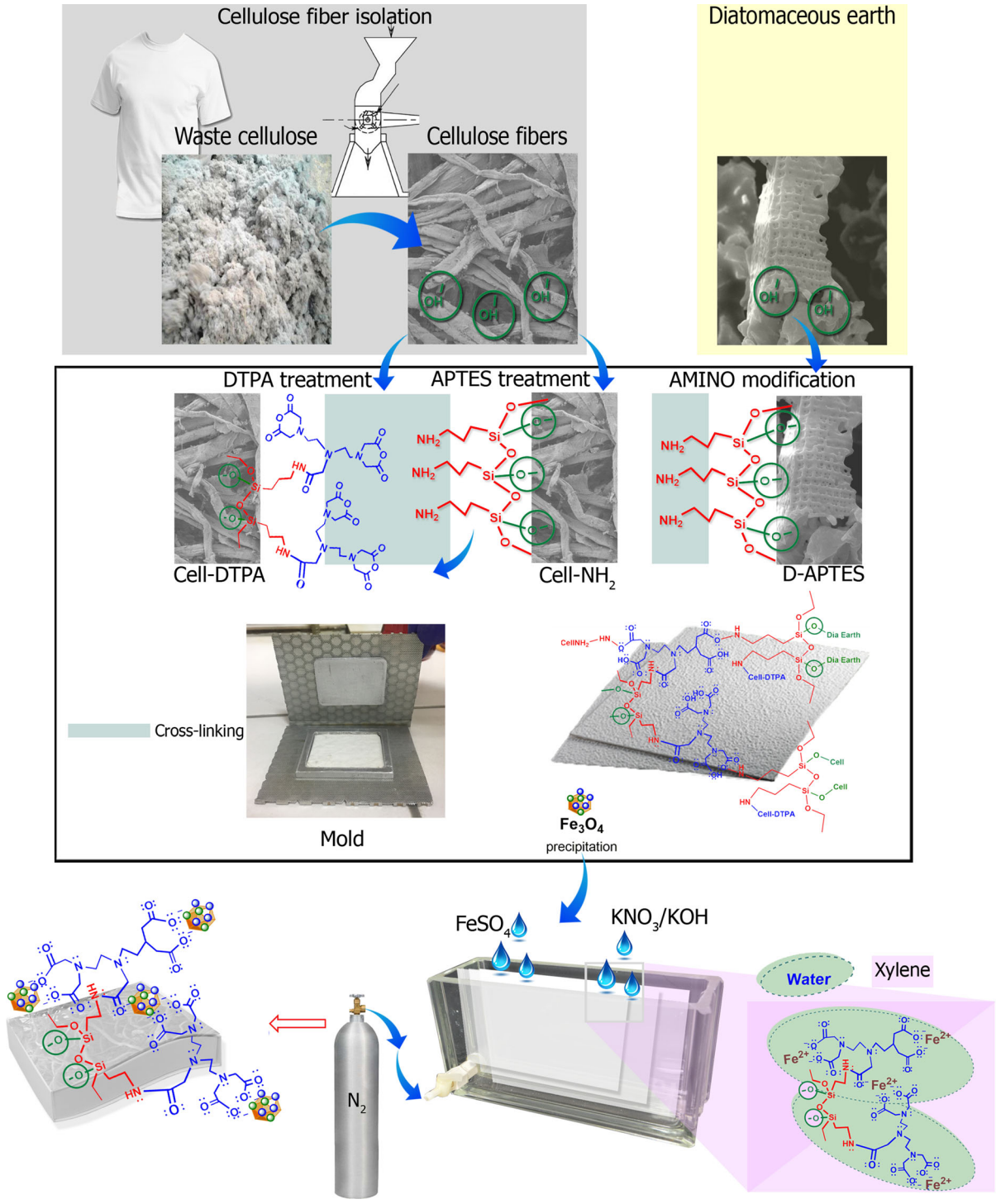

Fig. 2 Schematic presentation of the production steps in the course of Cell-MG hybrid membrane production

Table 2 Mechanical characteristics of cellulose-based membranes

Types of membranes	Stress at break (MPa)	Maximum strain (%)	Young's modulus (MPa)
Cell fibre	4.75	1.42	334.5
Cell-NH_2	4.45	1.41	315.6
Cell-DTPA	3.80	1.14	333.3
Cell-COOH membrane	5.30	1.92	276.0
Cell-MG hybrid membrane	4.05	1.36	297.8

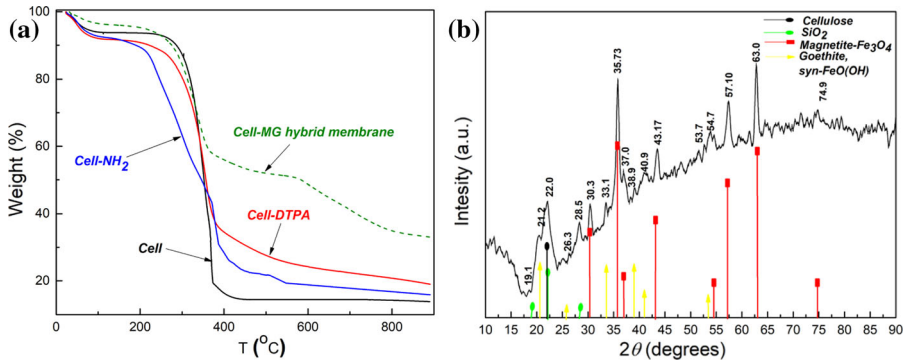

Fig. 3 Thermogravimetric analysis (TGA) of Cell, Cell-NH_2, Cell-DTPA and Cell-MG hybrid membrane (**a**) and XRD pattern of Cell-MG hybrid membrane (**b**)

Surface morphology analysis

The results from SEM analyses of surface morphology of the non-modified Cell membrane and Cell-MG adsorbent and diatomite are given in Figs. 5 and S6, respectively.

From Fig. 5a, a disordered structure of the non-modified fibre could be observed, which was purified and activated to obtain more active surface in the further processes of modification with APTES and DTPA. Controlled precipitation of MG on Cell-COOH membrane provides uniform distribution of deposit with increased surface, i.e. larger number of active sites for pollutant binding. The surface morphology of the hybrid adsorbent was similar to Cell fibres, suggesting that the precipitation of magnetite on the cellulosic matrix was evenly distributed and not affected the surface morphology of the cellulose.

Adsorption study

Influence of solution pH on adsorption efficiency

The most influential factors on the adsorption behaviour are pH-dependent ionic speciation and surface ionization. Results of pH_{PZC} determination (Table 1) suggest high removal potential of cations at $pH > pH_{PZC}$, while the opposite occurs for oxyanions. The pH-dependent ions speciation was performed using MINTEQ software, and the result is presented in Fig. S7. According to these data, and the results from the comprehensive study of pH-dependent adsorption of cations (Fig. S8) and oxyanions (Fig. S9) the optimal pH 7 for cation and 6 for oxyanions was selected. Selection of optimal pH provides achievement of high capacity, adsorbent stability, and using a wide range of real water without prior adjustment of inlet pH. Detailed analysis is given in Supplementary material.

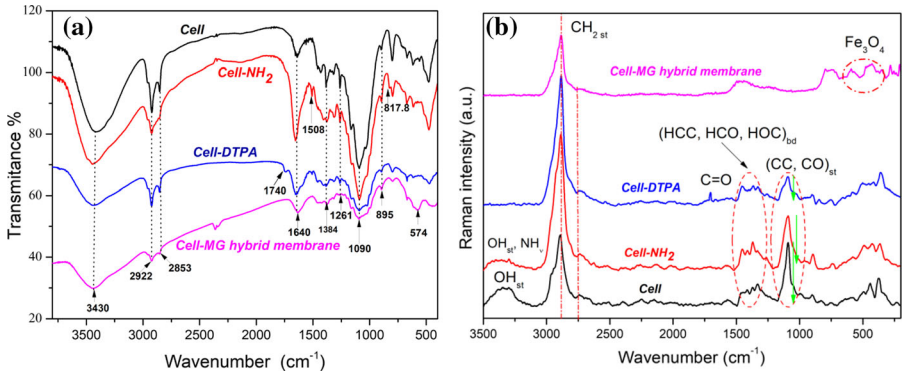

Fig. 4 FTIR (**a**) and Raman (**b**) spectra of Cell, Cell-NH_2, Cell-DTPA fibres and Cell-MG

Adsorption isotherms

The adsorption capacities were determined from equilibrium data at optimal operational pH. In order to understand the benefits of Cell-COOH modification with MG both adsorbents, Cell-COOH and Cell-MG were used in a comparative adsorption experiment. The equilibrium adsorption data were fitted with the four most frequently used isotherm models: Langmuir Eq. (S5), Freundlich Eq. (S6), Temkin Eq. (S9), and Dubinin–Radushkevich Eq. (S8). The adsorption capacity of Cell-COOH membrane, fitted by using Langmuir isotherm, showed acceptable capacities of 35.89 and 79.48 mg g^{-1} for $Ni^{2+}$and Pb^{2+}, respectively (Table S5), what means that de-protonation of the carboxylic groups provides active coordination sites for cations (at pH > 3.9). Significantly lower capacity for $HCrO_4^-/CrO_4^{2-}$ and $H_2AsO_4^-/HAsO_4^{2-}$ (61 and 69% lower, respectively) was obtained. The adsorption data for Cell-MG are presented in Tables 3 and S6–S9.

High monolayer coverage capacities (q_m) for all studied ions, obtained using Langmuir isotherm model (Table 3), increase with the temperature increase. Moreover, higher values of the Langmuir constant (K_L), that reflect the sorption affinity, were obtained for Pb^{2+} and $HAsO_4^{2-}/H_2AsO_4^-$oxyanions at all temperatures. The calculated R_L from Langmuir model fitting indicates favourable adsorption process (Tables S6–S9).

As can be seen from Table S7, the Freundlich isotherm is the best fitting one for the Pb^{2+} adsorption. The parameter n was in the range of 1–10, indicating a favourable adsorption process. Since the Freundlich constant K_F is an approximate indicator of adsorption capacity, and comparing to the values obtained by using Langmuir model, it clearly shows a good adsorption capacity of Cell-MG for Pb^{2+} ions.

As shown in Table S9 for As(V), Freundlich adsorption intensity parameter 1/n was in range 0.646–0.660, which proved that values of n between 2 and 10 indicated good adsorption. Irrespectively to the lower values of the correlation coefficients obtained by using Temkin and Dubinin–Radushkevich models, some information on the studied systems could be obtained. In the Temkin isotherm, A_T is the bond constant that represents the maximum binding energy (dm^3mg^{-1}). The mean B indexes, which relate to the heat of adsorption, indicate physical adsorption for all ions. According to Dubinin–Radushkevich isotherm model fitting and determination of the mean free energy, chemical ion-exchange dominates for Ni^{2+}, Cr(VI) and for As(V) ($8 < E_a < 16$ kJmol^{-1}), while physical process is a main contributor for Pb^{2+} ($E_a < 8$ kJmol^{-1}).

Thermodynamic parameters of adsorption

The Gibbs free energy (ΔG^{Θ}), enthalpy (ΔH^{Θ}) and entropy (ΔS^{Θ}) calculated from Van't Hoff equation [Eqs. (S10) and (S11)] were used for the analysis of thermodynamic aspect of the adsorption process. The calculated thermodynamic parameters are presented in Table 4.

Negative ΔG^{Θ} values demonstrate spontaneity and more favorable processes at higher temperatures. The positive values of the enthalpy (ΔH^{Θ}) indicate an endothermic nature of adsorption with beneficial influence of temperature increase on the capacity. The difference in ΔH^{Θ} between analysed ions was

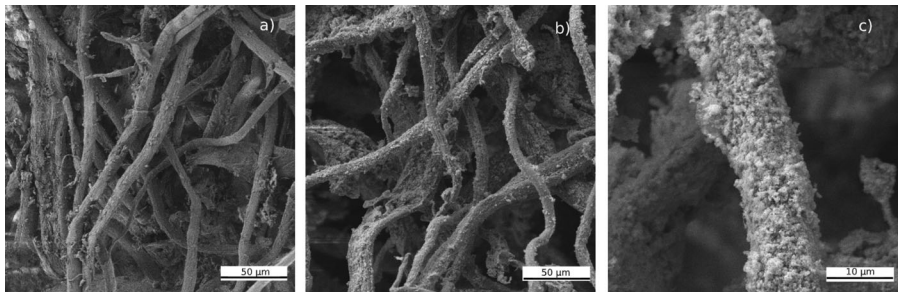

Fig. 5 SEM images of cell based membrane (**a**), and Cell-MG hybrid membrane (**b**, **c**)

noted, with the lowest value found for As(V). The highest hydration enthalpy of Ni^{2+} (Table S10) causes higher contribution to positive enthalpy change. Thus, the mutual contribution of endothermic nature of desolvation process and creation of surface complexes/bonding structure are the main influencing factors to ΔH^{Θ} changes.

Positive values of entropy change mean higher randomness of the system at equilibrium. Different processes in the course of adsorption contribute at different extent to ΔS^{Θ} change: highly arranged water in ion hydration shell (ion/hydrogen-bonding interaction) and formation of surface coordination complexes, i.e. geometric adaption of surface complex, decreased freedom of the system contributing to entropy decrease. On the other hand, release of water/proton from hydration shell and the adsorbent surface contributes to ΔS^{Θ} increase. Accordingly, higher entropy means better stability of a complex and more feasible process.

Adsorption kinetics

The determination of adsorption rate and the rate-controlling steps help in analysis of adsorption mechanism. The different kinetic rate law equations were used to model the experimental data: the pseudo-first order (Lagergren), the pseudo-second order (PSO), i.e. the Ho–McKay model, the second-order rate and the Roginsky–Zeldovich–Elovich equation, Eqs. (S12)–(S18), respectively, applying both linear and non-linear least-squares methods (Kaygusuz et al. 2015). The best correlation was obtained using non-linear fitting with PSO equation (Table S11). Also, the PSO rate constants at 25, 35 and 45 °C provide data for determination of activation energy [Eq. (S19)], and the obtained results are given in Table 5.

The results from Tables 4 and 5 suggest that both the concentration of adsorbate and Cell-MG surface functionalities are involved in the rate-controlling step, and the physisorption and chemisorption processes are involved to a different extent. A known fact that smaller (Table S10) and less solvated ions travel faster through the porous adsorbent structure is in agreement with results given in Table 3 and data from Table S10. Also, the results obtained by fitting the kinetic data with intra-particle Weber–Morris (W–M) (Eq. (S20), Dunwald–Wagner (D–W) [Eqs. (S21–S23)], and Homogenous Solid Diffusion (HSDM) model [Eqs. (S24–S26)] were used for evaluation of the rate-limiting step (Table 6).

Values of intercept C (mg g^{-1}) provide data about the thickness of the boundary layer. The boundary layer effect is stronger if the intercept is larger. If the plot passes through the origin, then the rate-limiting process is only the intra-particle diffusion, if not, some other mechanism along with intra-particle diffusion is involved. According to the results of W–M plot from Table 6, a high value of W–M constant C indicates that intra-particle diffusion is not the only rate-limiting step and that the influence of the other factors determines the effectiveness of the overall process. The value for k_{p1} shows the fast adsorption process of ions, in that the Ni^{2+}, Pb^{2+},Cr(VI) and As(V) ions are transferred by film diffusion. The value k_{p2} describes the part of the process whereby the ions are slowly diffusing inside the pores and adsorbing onto liquid/adsorbent interface. From the intra-particle diffusion rate constants listed in Table 6, it can be concluded that both film and intra-particle diffusion processes control the rate of adsorption with the dominance of the latter.

Table 3 The results of non-linear fitting using Langmuir isotherm model for Ni^{2+}, Pb^{2+}, Cr(VI) and As(V) adsorption onto Cell-MG hybrid membrane

Langmuir model	q_m (mg g^{-1}) (°C)	K(dm^3 mg^{-1})	K_L(dm^3 mol^{-1})	R^2
Ni^{2+}				
25	88.23	0.329	19,337.3	0.997
35	89.62	0.439	25,813.3	0.998
45	91.77	0.656	38,550.7	0.998
Pb^{2+}				
25	100.70	0.983	203,714.0	0.996
35	103.90	1.149	238,081.0	0.995
45	104.30	1.359	281,588.0	0.992
Cr(VI)				
25	95.80	0.423	22,045.5	0.992
35	99.70	0.564	29,344.0	0.997
45	111.20	0.817	42,516.8	0.992
As(V)				
25	78.17	5.062	379,288.6	0.996
35	79.73	6.040	452,536.7	0.993
45	81.32	6.836	512,125.7	0.990

Desorption

In a last few decades, significant improvements are being reported in the development of suitable and effective adsorbents for heavy metals removal, but less attention was paid to desorption efficiency and effluent water disposal. Proper selection of desorption agent and design of overall technology which has a minimal negative effect to adsorbent properties and environment is of utmost importance. Adsorbent performance can be diminished during the usage (i.e. incomplete desorption, precipitation and pore clogging, destruction of active sites etc.), in that way effects on the number of desorption cycles. Because of that the goal is to obtain the adsorbent with the lowest degree of deterioration after desorption. One task on the environmental aspect was solved by using biodegradable membranes, while another one, related to the disposal of polluted effluent water, needs yet to be solved. Regeneration efficiency and the number of regeneration cycles of Cell-MG, i.e. a number of adsorption/desorption processes, greatly improves of both economic and environmental indicators. Thus, optimization of the reusability was performed in a relation to desorption parameters such as regenerator type, concentration and operational time, as well as effluent water processing (ion exchange, precipitation, filtration, etc.), pH and concentration of reagent used for treatment. With the aim of applying the optimal desorption agent, in this study, a number of different agents (Supplementary material) have been tested. In a processes of As(V), Cr(VI) and cations desorption both alkaline and acidic regenerators were used, and it was found that their performance depended on the adsorbate/surface functionalities bonding types/strength.

The best desorption system contained sodium hydrogen carbonate ($NaHCO_3$, 4%) and salt (NaCl, 2%) for cation, while NaOH (4%) and NaCl (2%) for oxyanions. The obtained results for Ni^{2+}, Pb^{2+},

Table 4 Calculated Gibbs free energy, enthalpy and entropy for Cell-MG hybrid membrane

Ion	ΔG^{Θ} (kJ mol^{-1})			ΔH^{Θ} (kJ mol^{-1})	ΔS^{Θ} (J mol^{-1} K^{-1})	R^2
	298 K	308 K	318 K			
Ni^{2+}	− 34.42	− 36.32	− 38.56	27.15	206.32	0.987
Pb^{2+}	− 40.26	− 42.01	− 43.81	12.76	177.78	0.998
Cr(VI)	− 34.75	− 36.64	− 38.81	25.85	203.11	0.991
As(V)	− 41.80	− 43.65	− 45.40	11.86	180.03	0.993

$CrO_4^{2-}/HCrO_4^-$ and $HAsO_4^{2-}/H_2AsO_4^-$ ions, showed low reduction in adsorption efficiency for 18%, 22%, 19% and 25%, respectively, after third cycle. The pH adjustment before the next adsorption cycle was performed by simple DW washing.

Concentrated pollutants in effluent water are environmentally threatening agents and they need to be properly landfilled. Thus, design of the technology for their treatment into a material of appropriate hazardous characteristics suitable for landfilling was a main focus of a subsequent investigation.

Heavy metal hydroxide precipitation is the common simple and low-cost and straightforward method employed. Chemical precipitation, using MgO, $Ca(OH)_2$ and CaO, was conducted to treat effluent water solution. The optimum conversion of Cr(VI) to Cr(III), using ferrous sulfate, was performed at pH ~ 2.1 (Mirbagheri and Hosseini 2005). The minimum solubility for Cr(III), lead and nickel hydroxides are in the range 7.8–8.5, 8.3–8.9 and 10.4–10.8. The maximum precipitation of Cr(III) was achieved at pH 8.6, with the addition of $Ca(OH)_2$, as similarly found in the literature at 8.7 (Mirbagheri and Hosseini 2005). When treating a solution containing nickel with CaO, it is necessary to provide pH value higher than 11, to cause precipitation (Brbooti et al. 2011), thus was a satisfying nickel removal (more than 97.8%) accomplished. Lead precipitation (99.1%) with $Ca(OH)_2$ was performed at pH ~ 12 according to the previously described methodology (Kavak 2013).

For solutions treated with MgO (at pH 8–10), the good removal efficiencies were also achieved in the range of 96.2–98.6%. When MgO was used as the precipitating agent for Cr(VI), Ni^{2+} and Pb^{2+}, the optimum pH was 8.2, 9.6 and 9.4, respectively, which was close to the results published by Brbooti et al. (2011). By using MgO the dense, easily separable and dewatered sludge was obtained. Oppositely, voluminous and low settling capability was obtained with CaO.

Valuable technology applied in the processes relates to desorption solution treatment with iron(III) chloride or $Ca(OH)_2$ (Budimirović et al. 2017), or their combination. Precipitation of As(V) with lime is a valuable method, especially as a pretreatment step where at properly adjusted condition the large quantity of pollutant could be separated. A variety of calcium arsenates salts precipitated by lime addition at different settling conditions, and their structure and properties depended mainly on the pH and the Ca/As molar ratios. The dissolution experiments, as the long-term stability parameters, indicated that the predominant compound formed at the Ca/As(V) ratio 2.0 was $Ca_4(OH)_2(AsO_4)_2{\cdot}4H_2O$, which after 100 days of dissolution experiment showed very low concentration of As(V) ($5.6{\cdot}10^{-6}$ mol/L) at 25 °C and final pH value of 13.1 (Zhu et al. 2006). It means that proper selection of precipitation condition, i.e. molar ratio Ca/As(V) and pH 7, provided 99.2% As(V) removal with high stability of material obtained. In order to satisfy MPC values, prescribed by WHO, reverse osmosis should be unavoidably applied as a final purification step.

Table 5 PSO model parameters and activation energy for the adsorption of Ni^{2+}, Pb^{2+}, Cr(VI) and As(V) ions on Cell-MG hybrid membrane at 25, 35 and 45 °C

	T (°C)	q_e (mg g^{-1})	k_2(g (mg min)$^{-1}$)	R^2	*Ea* (kJ/mol)
Ni^{2+}	25	82.87	0.0065	0.999	6.658
	35	85.65	0.0071	0.999	
	45	88.39	0.0077	0.999	
Pb^{2+}	25	89.18	0.0026	0.992	9.645
	35	91.83	0.0029	0.993	
	45	94.54	0.0033	0.994	
Cr(VI)	25	97.26	0.0031	0.994	14.797
	35	99.25	0.0037	0.997	
	45	101.28	0.0045	0.998	
As(V)	25	58.95	0.0023	0.998	10.250
	35	59.39	0.0026	0.999	
	45	59.59	0.0030	0.999	

Table 6 Kinetic parameters of the W–M, D–W and HSDM models for the adsorption of Ni^{2+}, Pb^{2+}, Cr(VI) and As(V) ions on Cell-MG hybrid membrane

Intra-particle diffusion	Constants	Ni^{2+}	Pb^{2+}	Cr(VI)	As(V)
Weber–Morris (step 1)	k_{p1} (mg g^{-1} $min^{-0.5}$)	4.223	4.412	2.077	3.817
	C (mg g^{-1})	53.613	46.104	64.613	21.905
	R^2	0.997	0.995	0.969	0.977
Weber–Morris (step 2)	k_{p2} (mg g^{-1} $min^{-0.5}$)	0.858	0.400	1.165	0.168
	C (mg g^{-1})	74.094	83.309	84.219	54.118
	R^2	0.970	0.996	0.986	0.994
Dunwald–Wagner	K	0.038	0.036	0.033	0.013
	R^2	0.982	0.905	0.931	0.804
Homogenous solid diffusion model	Ds	4.07×10^{-11}	3.96×10^{-11}	3.61×10^{-11}	$1.49 \cdot 10^{-11}$
	R^2	0.979	0.918	0.933	0.799

Monolayer model for single-compound adsorption and adsorption mechanism

Monolayer model for single-compound adsorption is based on a claim that studied ions, ether cations or oxyanions, are adsorbed with one energy that describes their interaction with the active groups on the surface of adsorbent (Sellaoui et al. 2017a). Adsorption energy (ε) can be calculated according to the Eq. (S27) (Sellaoui et al. 2017b). Pseudo-reactions given in Eqs. (1)–(3) describe that each adsorption site accommodates one ion (Sellaoui et al. 2017a, b):

$$n\mathrm{Ni}^{2+}/\mathrm{Pb}^{2+} + \mathrm{S} \rightleftarrows \mathrm{Ni}^{2+}/\mathrm{Pb}^{2+}n\mathrm{S} \quad (1)$$

$$n\mathrm{HCrO}_4^-/\mathrm{H}_2\mathrm{AsO}_4^- + \mathrm{S} \rightleftarrows \mathrm{HCrO}_4^-/\mathrm{H}_2\mathrm{AsO}_4^- n\mathrm{S} \quad (2)$$

$$n\mathrm{CrO}_4^{2-}/\mathrm{HAsO}_4^{2-} + \mathrm{S} \rightleftarrows \mathrm{CrO}_4^{2-}/\mathrm{HAsO}_4^{2-} n\mathrm{S}, \quad (3)$$

where S is the receptor site of the adsorbent (Fe_3O_4), $Ni^{2+}/Pb^{2+}nS$, $HCrO_4^-/H_2AsO_4^-nS$ and $CrO_4^{2-}/HAsO_4^{2-}nS$ represent formed monodentate or bidentate complexes of cations or oxyanions with Fe_3O_4 modified hybrid Cell-membranes, and n represents the number of the bonded ions per one Fe_3O_4 site. The partition function of one identical site (Z_{gc}) and the monolayer model for single-compound adsorption are described by Eqs. (S28)–(S30). Different values for the parameters for single-compound adsorption of Ni^{2+}, Pb^{2+}, $HCrO_4^-/CrO_4^{2-}$ and $H_2AsO_4^-/HAsO_4^{2-}$ ions on Cell-MG membranes are presented in Table 7.

The determination of the number of ions that interact with one Fe_3O_4 receptor site (–FeOH) provides valuable knowledge complementing the detection/conclusions for complex formation phenomena obtained from the isothermal adsorption study. If the number of the complexed ions per –FeOH receptor is lower than 1, the ions are multi-link connected (interact with at least two sites). If the n is higher than 1, the –FeOH site is occupied minimum by one ion (Sellaoui et al. 2017a, b). In the presented study, for the investigated single-compound systems, adsorption of $HCrO_4^-/CrO_4^{2-}$ on Fe_3O_4 modified hybrid Cell membranes, the values of the n higher than 1 are obtained at all investigated temperatures. It confirms that the main mechanism represents an interaction of two ions per one active –FeOH site, which is in accordance with the creation of monodentate mononuclear complexes (Zach-Maor et al. 2011; Johnston and Chrysochoou 2014). The opposite was found for Ni^{2+} and Pb^{2+} cations, and for $H_2AsO_4^-/HAsO_4^{2-}$ oxyanions. The parameter n slightly increases with temperature. Lower values than 1 are obtained for Ni^{2+} and Pb^{2+} ions, which confirms that the main mechanism of the removal of Ni^{2+} and Pb^{2+} ions occurs via an exchange of metal ions Ni^{2+}/Pb^{2+} with H^+ ions at the surface hydroxyl groups –FeOH, producing $Ni^{2+}/Pb^{2+}(OH)^+$ ions that are bonded to another –FeOH site. Also, electrostatic interactions of a positively charged ion with an electron pair of hydroxyl groups could be of appropriate significance. In general, the possible mechanisms of formation of monodentate and

bidentate complexes of $H_2AsO_4^-$/$HAsO_4^{2-}$ oxyanions with a hydroxyl group on MG surface are presented in Fig. 6.

Additional consideration of the adsorption process by using FTIR spectroscopy is given in Supplementary material (Fig. S10). The shift of isoelectric point of goethite with specifically adsorbed anions to lower value (Table 1) and results of FTIR analysis (Fig. S10) confirmed the formation of inner-sphere surface complexes of As(V) anions onto MG surface.

Application of Cell-MG hybrid adsorbent for mining wastewater treatment

A study on the efficiency of mining wastewater treatment was performed, and results are given in Supplementary material. The obtained results indicate the general applicability of Cell-MG in a processing of wastewater purification with high concentration of pollutants.

Membrane performance with respect to dyes removal

Permeation properties

Results of the permeation properties of Cell-MG indicate low rejection capability with high molecular weight cut-off obtained for sodium alginate (Supplementary material). Due to this, the adsorption characteristic of Cell-MG membrane adsorption performances was further studied with respect to the efficiency of four dyes removal.

Adsorption removal of dyes

The number of specific interactions taking place at the solid–liquid interface contributes to a different extent in an overall adsorption mechanism. The knowledge of the most preferable interaction between surface functionalities/appropriate dye could help in design of the adsorbent surface/functionalities to obtain optimal affinity/selectivity with respect to the selected pollutants. In order to evaluate membrane performances in relation to four organic/textile dyes, i.e. MO, MB, RB5 and DR80, adsorption study was performed and the results are given in Table 8.

High value of q_m for MB at pH 7.5 indicates a high affinity of negatively charged adsorbent to cationic dye (at $pH > pH_{PZC}$), while the opposite is true for anionic dyes. The values of capacity relates to the number of sulfonic groups. The calculated geometry parameters (Table S14), hydrophilicity/lipophilicity parameters (Table S15), molecular electrostatic potential (Fig. S13) and molecular interaction fields computed for O and N1 probe (HBA and HBD probe, Fig. 7) (Goodford 1985; Pastor et al. 2000), were considered with respect to the adsorption performances.

The chosen energy cut-off, manually selected to − 4 and − 6 kcal/mol for O and N1 probes, respectively, provided a good visualization of the differences in H-bonding characteristics between 4 dyes. It has to be stressed that O and N1 probe MIFs located only HBD and HBA sites of a neutral part of molecules, while ionized SO_3^- groups were not accounted. The relative strength of strong electrostatic interactions between 4 dyes and the surface of adsorbent can be elucidated from the quantitative analysis of molecular surface (ESP maps; Fig. S13). The establishment of stronger intermolecular bonds with the adsorbent surface, indicated by molecular electrostatic potential (Fig. S13) and MIFs (Fig. 7), correlates with the higher q_m values, so the interplay between electrostatics and hydrogen bonding dyes/surface functionalities determines the adsorption mechanism and capacity as well. Thus, the selection of optimal pH was guided by calculated parameters. Also, determination of the molecular geometry confirms significance of specific intermolecular interactions, which prevail over the contribution of the size of molecule (Table S14). Large pore size of Cell-MG membrane (Fig. 5) provides a condition for the high adsorbate mobility independent to molecular size (Table S14). In general, capacity change follows the order of the intensity of adsorbate/adsorbent interactions (Table S14), and significantly depends on the number of present sulfonate group (Fig. S12). Such methodology is applicable in a predictive manner to perform the adequate design of adsorbent with desired properties.

Bed column study

A fixed-bed column study was carried out to consider the possible application of Cell-MG adsorbent for real application in a water purification processes. Such processes, considering the use of ion exchange resin or

Table 7 Values of adjustable parameters in the single-compound system for adsorption of Ni^{2+}, Pb^{2+}, $HCrO_4^-/CrO_4^{2-}$ and $H_2AsO_4^-/HAsO_4^{2-}$ ions

Ni^{2+}						Pb^{2+}			
	T (K)	ε (KJ mol^{-1})	Q_{sat} (mg g^{-1})	N_M* (mg g^{-1})	n	ε (KJ mol^{-1})	Q_{sat} (mg g^{-1})	$N_M{}^*$ (mg g^{-1})	n
Cell-MG	298	8.678	89.18	66	0.814	7.825	83.43	52	0.980
	308	8.745	91.83	64	0.878	7.85	85.92	51	0.985
	318	8.848	94.54	61	0.937	7.869	88.41	50	0.994
$HcrO_4^-/CrO_4^{2-}$						$H_2AsO_4^-/HAsO_4^{2-}$			
	T (K)	ε (KJ mol^{-1})	Q_{sat} (mg g^{-1})	$N_M{}^*$ (mg g^{-1})	n	ε (KJ mol^{-1})	Q_{sat} (mg g^{-1})	$N_M{}^*$ (mg g^{-1})	n
Cell-MG	298	8.828	97.261	66	1.106	8.212	47.17	51	0.481
	308	8.916	99.248	63	1.173	8.224	47.57	50	0.489
	318	9.052	101.286	61	1.182	8.261	47.77	49	0.516

*N_M is the density of receptor site, and Q_{sat} is the heavy metal ion/oxyanion equilibrium adsorption capacity

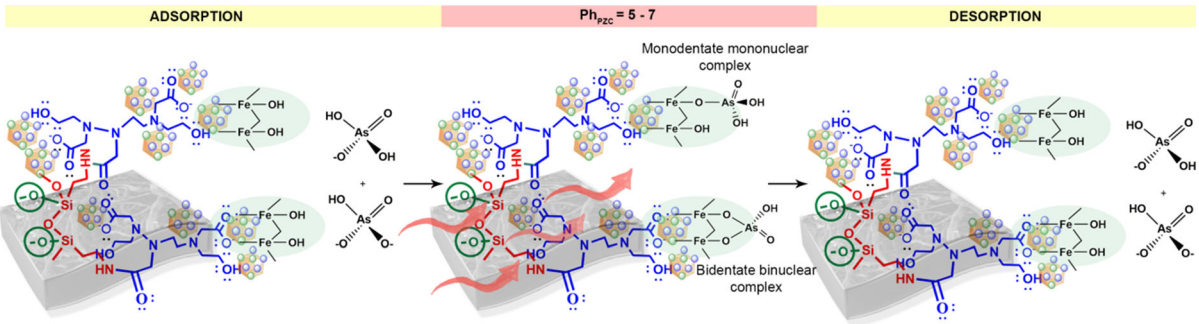

Fig. 6 Mechanisms of formation for monodentate and bidentate complexes

adsorbent, are limited by several factors: the time-dependent pressure drop across the adsorbent bed, which may increase over time due to media deformation and plugging and slow pore ion diffusion (internal) inside the resin, i.e. pore network, which could require generally long residence times. All of these factors determine adsorption efficiency i.e. the exhaustion of surface adsorption site. In order to overcome the performance issues of ion-exchange resin, the use of membrane offer opportunities to establish higher volumetric transport due to a lower diffusional resistance, i.e. a faster ion transport inside the pore to reach adsorption sites/functional groups and yield higher capacity. Response Surface Method was applied in order to rationalize the number of experiments and to select optimal operational parameters related to heavy metal ions column adsorption. The operational values (flow rate and concentration of Pb^{2+} in the medium) of the selected variables are shown in Table S16, and contour diagram which represent relation between concentration of Pb^{2+} and flow rate of influent water *versus* capacity are shown in Fig. S14.

The operational performance of Cell-MG in a dynamic mode requires determination of the breakthrough curve (Figs. S15-S18), and thus the calculation of the capacity was performed (Tables 9, 10). Details on the models usually used for the evaluation of adsorption efficiency, performances and applicability of the adsorbents for operations at a laboratory and industrial level, such as Yoon–Nelson Eq. (S35), Bohart–Adams Eq. (S36) and Modified dose–response model Eq. (S37), are given in Supplementary material.

A mathematical model (*Clark model*) was used to examine kinetics and mass-transfer aspects of the dynamic removal of Ni^{2+}, Pb^{2+}, Cr(VI) and As(V),

Eq. (S39)–(S41). The correlation between the predicted and experimental results indicates high applicative potential of Cell-MG in a real water purification system.

Overview of adsorption capacities and kinetic data of cellulose-based adsorbents

Adsorption capacities for Pb^{2+} ions by using cellulose-based adsorbents show improving results from 10.2 mg g^{-1} on non-modified cellulose (CNF-OH), 20–40 mg g^{-1} for macro and micro cellulose, 44.6 mg g^{-1} for cellulose microfiber, reaching 70.5 mg g^{-1} for cellulose acetate/polycaprolactone reinforced nanostructured membrane, and up to 98 mg g^{-1} for grafted copolymer of cellulose (Table S18). These results were obtained with relatively high initial concentrations mostly from 100 to 300 mg dm^{-3}. The obtained q_{max} of Cell-COOH for Pb^{2+} ions reached 79.48 mg g^{-1} at 25 ° C and 83.28 mg g^{-1} at 45 °C. Even higher q_{max} values were obtained using Cell-MG (100.7 mg g^{-1} at 25 °C and 104.30 at 45 °C, Table 3). The adsorption capacity for Ni^{2+} with non-modified cellulose was calculated to be 11.2 mg g^{-1}. The maximum adsorption capacity of 18.44 mg g^{-1} for Ni^{2+} ions was obtained with β-cyclodextrin-cellulose/hemicellulose-based hydrogels with a very high initial concentration of 500 mg dm^{-3}, while PSO adsorption rate constant was relatively low, $k_2 = 0.26 \times 10^{-2}$ g mg^{-1} min^{-1} (Table S18). By using a grafted copolymer of cellulose, the adsorption capacity of 74.5 mg g^{-1} was obtained at initial concentration of 100 mg dm^{-3} and PSO $k_2 = 9.64 \times 10^{-3}$ g mg^{-1} min^{-1}. Cell-COOH from in this work reached value of 40.59 mg g^{-1}- adsorption capacity at 45 °C, while the obtained capacity for Cell-MG hybrid membrane was 91.77 mg g^{-1}. Values of Cr(VI) removal varied from 18.13 mg g^{-1} for regenerated cellulose membrane with the initial concentration of 100 mg dm^{-3}, 33.1 mg g^{-1} for peanut husk and 42.44 mg g^{-1} macadamia nutshell powder with initial concentration of 25 and 100 mg dm^{-3}, respectively (Table S18). High adsorption capacity values (171.5 mg g^{-1}) for Cr(VI) removal were obtained by using magnetic cellulose nanocomposite. The significantly higher adsorption capacities (95.8 mg g^{-1} at 25 °C up to 111.2 mg g^{-1} at 45 °C) of Cr(VI) ion removal were obtained for the as-prepared Cell-MG hybrid membrane (Table 3). For example, the adsorption capacities, q_{max} for As(V) ions found in the literature were 5.45 mg g^{-1} using cellulosic-ferric oxide system and 25.5 mg g^{-1} for cellulose nanofibrils (CNF) with initial concentration of 10 mg dm^{-3} at 25 °C and room temperature, respectively, (Table S18). The q_{max} values for As(V) ion removal obtained in this research using Cell-MG hybrid membrane were 61.9 mg dm^{-3} at 25 °C and 67.2 mg dm^{-3} at 45 °C. A comparison of

Table 8 The results of Langmuir isotherm model fitting for dyes adsorption (C_i[MO] = 27 mg dm^{-3}, pH 6;C_i[MB] = 30 mg dm^{-3}, pH 7.5; C_i[RB5] = 25 mg dm^{-3}, C_i[DR80] = 36 mg dm^{-3}, m/V = 125 mg L^{-1}, T = 298 K, pH 6)

Langmuir isotherm model (°C)	q_m(mg g^{-1})	K(dm^3 mg^{-1})	K_L(dm^3 mol^{-1})	R^2
MO				
25	71.596	0.65801	215,384.9	0.998
35	80.232	0.69942	228,940.2	0.998
45	88.905	0.77189	252,663.9	0.996
MB				
25	83.012	0.24174	77,320.5	0.985
35	101.179	0.20235	64,720.8	0.979
45	120.632	0.17838	57,054	0.969
RB5				
25	125.130	0.25326	251,180.3	0.978
35	130.780	0.25914	257,010.5	0.985
45	138.309	0.26089	258,750.4	0.993
DR80				
25	245.552	0.06590	90,487.6	0.972
35	260.117	0.07571	103,954.2	0.984
45	271.078	0.08981	123,317.6	0.988

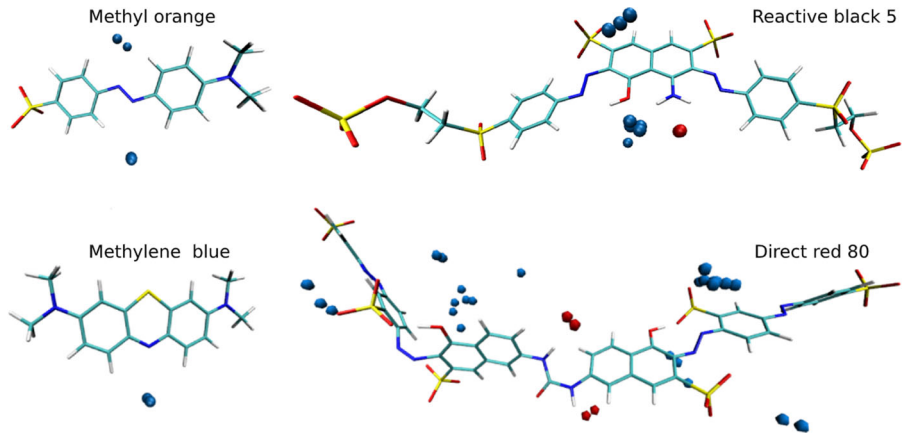

Fig. 7 Molecular interaction fields computed for O and N1 probe (HBA and HBD probe). Interaction energy cutoffs: − 4 kcal/mol for O and − 6 kcal/mol for N1 probe

Table 9 Bohart–Adams, Yoon–Nelson and Modified dose–response model fitting for Ni^{2+} and Pb^{2+}adsorption by Cell-MG ($C_i[Ni^{2+}]$ = 6.10 mg dm^{-3}; $C_i[Pb^{2+}]$ = 6.20 mg dm^{-3}; m_{ads} = 430 mg; t = 25 °C; pH = 7, BV = 0.8 cm^{-3})

Q	$cm^3\ min^{-1}$	Ni^{2+}			Pb^{2+}		
		0.5	1	1.5	0.5	1	1.5
EBCT	min	3.92	1.96	1.30	3.92	1.96	1.30
Bohart–Adams model							
k_{BA}	$dm^3\ mg^{-1}\ min^{-1}$	0.181	0.254	0.241	0.215	0.200	0.215
q_o	$mg\ g^{-1}$	80.240	80.409	80.251	84.056	80.992	78.438
R^2		0.990	0.980	0.960	0.996	0.997	0.993
Yoon–Nelson model							
k_{YN}	min^{-1}	0.203	1.564	0.983	2.675	1.242	0.889
θ	min	5.656	5.612	5.654	5.829	5.617	5.440
R^2		0.990	0.980	0.960	0.996	0.997	0.930
Modified dose–response model							
a		1.996	1.725	1.534	2.379	2.006	1.846
q_o	$mg\ g^{-1}$	89.161	92.435	89.629	91.531	84.517	75.901
R^2		0.534	0.572	0.641	0.612	0.673	0.740

maximum adsorption capacities and the rate constant of heavy metal ions/oxyanions removal of cellulose-based adsorbents reported in the literature with those obtained for Cell-MG indicates excellent adsorption performances of membranes obtained in this research. In addition, very high adsorption capacity values in both batch and fixed bed study under a high loading rate indicate promising applicability of the Cell-MG membrane.

Conclusion

In this study, the synthesized magnetite (MG) modified cross-linked carboxy functionalized cellulose membrane proved to be effective in a process of Ni^{2+}, Pb^{2+}, Cr(VI) and As(V) removal from water. Application of Box-Behnken experimental design in RSM provides successful synthesis of Cell-MG membrane and good prediction of the fixed-bed column results. The high adsorption capacities, calculated from Langmuir model fitting, obtained for aqueous solutions, wastewater from the mining industry and efficient dyes removal indicate the high performance of Cell-MG membrane. The results from adsorption

Table 10 Bohart–Adams, Yoon–Nelson and Modified dose–response model fitting for Cr(VI) and As(V) adsorption by Cell-MG (C_i[Cr(VI)] = 6.20 mg dm^{-3}; C_i[As(V)] = 5.00 mg dm^{-3};m_{ads} = 430 mg; t = 25 °C; pH = 6, BV = 0.8 cm^{-3})

Q	cm^3 min^{-1}	Cr(VI)			As(V)		
		0.5	1	1.5	0.5	1	1.5
EBCT	min	3.92	1.96	1.30	3.92	1.96	1.30
Bohart–Adams model							
k_{BA}	dm^3 mg^{-1} min^{-1}	5.763	5.958	5.758	4.70	6.463	7.363
q_o	mg g^{-1}	76.681	72.307	66.506	43.802	37.551	31.297
R^2		0.998	0.996	0.997	0.999	0.998	0.990
Yoon–Nelson model							
k_{YN}	min^{-1}	3.573	1.847	1.190	2.820	1.939	1.473
θ	min	5.318	5.015	4.612	3.139	2.691	2.243
R^2		0.998	0.996	0.997	0.999	0.998	0.990
Modified dose–response model							
a		2.096	1.963	1.732	2.763	2.510	1.940
q_o	mg g^{-1}	92.339	89.272	91.596	34.533	32.101	30.055
R^2		0.539	0.554	0.566	0.876	0.876	0.805

and kinetics study showed the high efficiency and usability of the obtained adsorbent. An adjusted porosity provides condition for a good overall kinetic and thus effective application in a flow system was achieved. The experimental data were fitted well applying the Bohart–Adams, Yoon–Nelson, Thomas and modified dose–response models. Besides, a successful valorization of waste cellulosic fibers as adsorbents and the use of RSM methods in order to reduce the number of experiments contributed to decrease of waste generation. Thus, the obtained results and applied methods were in accordance with the current environmental policies related to the development and implementation of the comprehensive technologies for waste management and environmental protection.

Acknowledgments The authors acknowledge financial support from Ministry of Education, Science and Technological development of the Republic of Serbia, Contract Nos. 451-03-68/2020-14/200026, 451-03-68/2020-14/200135, 451-03-68/2020-14/200325 and 451-03-68/2020-14/200288)

Compliance with ethical standards

Conflict of interest The authors declare that they have no conflict of interest.

Declaration of permission Permission for collecting the waste cellulosic material from the Belgrade landfill was received from the Public Utility Company for City Sanitation and waste collecting for the city of Belgrade—JKP "GRADSKA ČISTOĆA".

References

Ahangaran F, Hassanzadeh A, Nouri S (2013) Surface modification of Fe_3O_4@SiO_2 microsphere by silane coupling agent. Int Nano Lett 3:3–7. https://doi.org/10.1186/2228-5326-3-23

Arantes ACC, das Almeida CG, Dauzacker LCL et al (2017) Renewable hybrid nanocatalyst from magnetite and cellulose for treatment of textile effluents. Carbohydr Polym 163:101–107. https://doi.org/10.1016/j.carbpol.2017.01.007

Boyatzis SC, Velivasaki G, Malea E (2016) A study of the deterioration of aged parchment marked with laboratory iron gall inks using FTIR-ATR spectroscopy and micro hot table. Herit Sci 4:1–17. https://doi.org/10.1186/s40494-016-0083-4

Brbooti MM, Abid BA, Al-Shuwaiki NM (2011) Removal of heavy metals using chemicals precipitation. Eng Technol J 29:595–612

Budimirović D, Veličković ZS, Djokić VR et al (2017) Efficient As(V) removal by α-FeOOH and α-FeOOH/ α-MnO2 embedded PEG-6-arm functionalized multiwall carbon nanotubes. Chem Eng Res Des 119:75–86. https://doi.org/10.1016/j.cherd.2017.01.010

Dave PN, Chopda LV (2014) Application of iron oxide nanomaterials for the removal of heavy metals. J Nanotechnol. https://doi.org/10.1155/2014/398569

El Achaby M, El Miri N, Aboulkas A et al (2017) Processing and properties of eco-friendly bio-nanocomposite films filled with cellulose nanocrystals from sugarcane bagasse. Int J

Biol Macromol 96:340–352. https://doi.org/10.1016/j.ijbiomac.2016.12.040

ElSayed EE (2018) Natural diatomite as an effective adsorbent for heavy metals in water and wastewater treatment (a batch study). Water Sci 32:32–43. https://doi.org/10.1016/j.wsj.2018.02.001

Fakhre NA, Ibrahim BM (2018) The use of new chemically modified cellulose for heavy metal ion adsorption. J Hazard Mater 343:324–331. https://doi.org/10.1016/j.jhazmat.2017.08.043

Freire PTC, Barboza FM, Lima JA et al (2017) Raman spectroscopy of amino acid crystals. Raman Spectrosc Appl. https://doi.org/10.5772/65480

Goodford PJ (1985) A computational procedure for determining energetically favorable binding sites on biologically important macromolecules. J Med Chem 28:849–857. https://doi.org/10.1021/jm00145a002

Han ED, Park CW, Lee SH et al (2020) Polar molecule filtration using charged cellulose nanofiber membrane on the nanoporous alumina support for high rejection efficiency. Cellulose 27:2685–2694. https://doi.org/10.1007/s10570-019-02928-6

Hua M, Zhang S, Pan B et al (2012) Heavy metal removal from water/wastewater by nanosized metal oxides: a review. J Hazard Mater 211–212:317–331. https://doi.org/10.1016/j.jhazmat.2011.10.016

Johnston CP, Chrysochoou M (2014) Mechanisms of chromate adsorption on hematite. Geochim Cosmochim Acta 138:146–175

Kamel S, Hassan EM, El-Sakhawy M (2006) Preparation and application of acrylonitrile-grafted cyanoethyl cellulose for the removal of copper (II) ions. J Appl Polym Sci 100:329–334. https://doi.org/10.1002/app.23317

Kavak D (2013) Removal of lead from aqueous solutions by precipitation: statistical analysis and modeling. Desalin Water Treat 51:1720–1726. https://doi.org/10.1080/19443994.2012.714652

Kaygusuz H, Uzaşçı S, Erim FB (2015) Removal of fluoride from aqueous solution using aluminum alginate beads. Clean: Soil, Air, Water 43:724–730. https://doi.org/10.1002/clen.201300632

Khraisheh MAM, Al-degs YS, Mcminn WAM (2004) Remediation of wastewater containing heavy metals using raw and modified diatomite. Chem Eng J 99:177–184. https://doi.org/10.1016/j.cej.2003.11.029

Li Y, Xiao H, Chen M et al (2014) Absorbents based on maleic anhydride-modified cellulose fibers/diatomite for dye removal. J Mater Sci 49:6696–6704. https://doi.org/10.1007/s10853-014-8270-8

Li Y, Chen MD, Wan X et al (2017) Solvent-free synthesis of the cellulose-based hybrid beads for adsorption of lead ions in aqueous solutions. RSC Adv 7:53899–53906. https://doi.org/10.1039/c7ra09592a

Li Y, Jiang Y, Deng Q et al (2020) Insights into performance, structure-property relationship and adsorption mechanism to efficiently remove Ni^{2+} by corn stalk cellulose functionalized with amino groups. Cellulose. https://doi.org/10.1007/s10570-020-03098-6

Lu S, Hu J, Chen C et al (2017) Spectroscopic and modeling investigation of efficient removal of U(VI) on a novel magnesium silicate/diatomite. Sep Purif Technol 174:425–431. https://doi.org/10.1016/j.seppur.2016.09.052

Luo X, Lei X, Cai N et al (2016) Removal of heavy metal ions from water by magnetic cellulose-based beads with embedded chemically modified magnetite nanoparticles and activated carbon. ACS Sustain Chem Eng 4:3960–3969. https://doi.org/10.1021/acssuschemeng.6b00790

Mirbagheri SA, Hosseini SN (2005) Pilot plant investigation on petrochemical wastewater treatment for the removal of copper and chromium with the objective of reuse. Desalination 171:85–93. https://doi.org/10.1016/j.desal.2004.03.022

Munajad A, Subroto C, Suwarno (2018) Fourier transform infrared (FTIR) spectroscopy analysis of transformer paper in mineral oil–paper composite insulation under accelerated thermal aging. Energies. https://doi.org/10.3390/en11020364

Nouri M, Marjani A (2019) Surface modification of a cellulose acetate membrane using a nanocomposite suspension based on magnetic particles. Cellulose 26:7995–8006. https://doi.org/10.1007/s10570-019-02639-y

O'Connell DW, Birkinshaw C, O'Dwyer TF (2008) Heavy metal adsorbents prepared from the modification of cellulose: A review. Bioresour Technol 99:6709–6724. https://doi.org/10.1016/j.biortech.2008.01.036

Pastor M, Cruciani G, Mclay I et al (2000) GRid-independent descriptors (GRIND): a novel class of alignment-independent three-dimensional molecular descriptors. J Med Chem 43:3233–3243

Popovic DM, Milosavljevic V, Zekic A et al (2011) Raman scattering analysis of silicon dioxide single crystal treated by direct current plasma discharge. Appl Phys Lett 98:10–13. https://doi.org/10.1063/1.3543838

Pramanik K, Sarkar P, Bhattacharyay D (2019) 3-Mercaptopropanoic acid modified cellulose filter paper for quick removal of arsenate from drinking water. Int J Biol Macromol 122:185–194. https://doi.org/10.1016/j.ijbiomac.2018.10.065

Rafieian F, Jonoobi M, Yu Q (2019) A novel nanocomposite membrane containing modified cellulose nanocrystals for copper ion removal and dye adsorption from water. Cellulose 26:3359–3373. https://doi.org/10.1007/s10570-019-02320-4

Ren C, Ding X, Li W et al (2017) Highly efficient adsorption of heavy metals onto novel magnetic porous composites modified with amino groups. J Chem Eng Data 62:1865–1875. https://doi.org/10.1021/acs.jced.7b00198

Salih SS, Ghosh TK (2018) Highly efficient competitive removal of Pb(II) and Ni(II) by chitosan/diatomaceous earth composite. J Environ Chem Eng 6:435–443. https://doi.org/10.1016/j.jece.2017.12.037

Sellaoui L, Dotto GL, Ben LA, Erto A (2017a) Interpretation of single and competitive adsorption of cadmium and zinc on activated carbon using monolayer and exclusive extended monolayer models. Environ Sci Pollut Res 24:19902–19908. https://doi.org/10.1007/s11356-017-9562-8

Sellaoui L, Edi Soetaredjo F, Ismadji S et al (2017b) New insights into single-compound and binary adsorption of copper and lead ions on treated sea mango shell:

experimental and theoretical studies. Phys Chem Chem Phys 19:25927–25937. https://doi.org/10.1039/c7cp03770h

Shebanova ON, Lazor P (2003) Raman study of magnetite (Fe_3O_4): laser-induced thermal effects and oxidation. J Raman Spectrosc 34:845–852. https://doi.org/10.1002/jrs.1056

Sheng G, Wang S, Hu J et al (2009) Adsorption of Pb(II) on diatomite as affected via aqueous solution chemistry and temperature. Colloids Surfaces A Physicochem Eng Asp 339:159–166. https://doi.org/10.1016/j.colsurfa.2009.02.016

Sun J, Liu X, Peng L (2013) The research progress of the modified cellulose magnetic microspheres adsorption of heavy metal. Adv Mater Res 675:289–295. https://doi.org/10.4028/www.scientific.net/AMR.675.289

Sun X, Yang L, Li Q et al (2014) Amino-functionalized magnetic cellulose nanocomposite as adsorbent for removal of Cr(VI): synthesis and adsorption studies. Chem Eng J 241:175–183. https://doi.org/10.1016/j.cej.2013.12.051

Szymańska-Chargot M, Cybulska J, Zdunek A (2011) Sensing the structural differences in cellulose from apple and bacterial cell wall materials by raman and FT-IR spectroscopy. Sensors 11:5543–5560. https://doi.org/10.3390/s110605543

Tang SCN, Lo IMC (2013) Magnetic nanoparticles: essential factors for sustainable environmental applications. Water Res 47:2613–2632. https://doi.org/10.1016/j.watres.2013.02.039

Tkacheva NI, Morozov SV, Grigor'ev IA et al (2013) Modification of cellulose as a promising direction in the design of new materials. Polym Sci Ser B 55:409–429. https://doi.org/10.1134/s1560090413070063

Vadakkekara GJ, Thomas S, Nair CPR (2019) Maleic acid modified cellulose for scavenging lead from water. Int J Biol Macromol 129:293–304. https://doi.org/10.1016/j.ijbiomac.2019.02.037

Vítek P, Klem K, Urban O (2017) Application of Raman spectroscopy to analyse lignin/cellulose ratio in Norway spruce tree rings. Beskydy 10:41–48. https://doi.org/10.11118/beskyd201710010041

Wiley JH, Atalla RH (1987) Raman spectra of celluloses James H. Wiley and Rajai H. Atalla. Am Chem Soc 226:151–168

Xu P, Zeng GM, Huang DL et al (2012) Use of iron oxide nanomaterials in wastewater treatment: a review. Sci Total Environ 424:1–10. https://doi.org/10.1016/j.scitotenv.2012.02.023

Zach-Maor A, Semiat R, Shemer H (2011) Adsorption–desorption mechanism of phosphate by immobilized nano-sized magnetite layer: interface and bulk interactions. J Colloid Interface Sci 363:608–614. https://doi.org/10.1016/j.jcis.2011.07.062

Zhu YN, Zhang XH, Xie QL et al (2006) Solubility and stability of calcium arsenates at 25 °C. Water Air Soil Pollut 169:221–238. https://doi.org/10.1007/s11270-006-2099-y